Journal of Solid State Chemistry **168,** 616–625 (2002)
doi:10.1006/jssc.2002.9759

Hybrid Molecular Materials Based upon Organic π-Electron Donors and Inorganic Metal Complexes. Conducting Salts of Bis(ethylenediseleno)tetrathiafulvalene (BEST) with the Octahedral Anions Hexacyanoferrate(III) and Nitroprusside

Miguel Clemente-León,* Eugenio Coronado,*,[1] José R. Galán-Mascarós,* Carlos Giménez-Saiz,* Carlos J. Gómez-García,* Jean M. Fabre,† G. A. Mousdis,‡ and G. C. Papavassiliou‡

*Instituto de Ciencia Molecular, Universidad de Valencia, Dr. Moliner 50, 46100 Burjasot Spain; †ENSCM / ESA- 5076. 8, rue de l'Ecole Normale F–34296 Montpellier, France; and ‡Theoretical and Physical Chemistry Institute, National Hellenic Research Foundation, 48 Vass. Constantinou Aven., 116 35 Athens, Greece

Received January 28, 2002; in revised form April 12, 2002; accepted April 19, 2002

The synthesis, structure and physical characterization of three new radical salts formed by the organic donor bis(ethylenediseleno)tetrathiafulvalene (BEDS-TTF or BEST) and the paramagnetic hexacyanoferrate(III) anion $[Fe(CN)_6]^{3-}$ or the photochromic nitroprusside anion $[Fe(CN)_5NO]^{2-}$ are reported: $(BEST)_4[Fe(CN)_6]$ (1), $(BEST)_3[Fe(CN)_6]_2 \cdot H_2O$ (2) and $(BEST)_2[Fe(CN)_5NO]$ (3). Salts 1 and 3 show a layered structure with alternating organic (β–type packing) and inorganic slabs. Salt 2 shows an original interpenetrated structure probably due to the unprecedented presence of $(BEST)^{2+}$ dications. The three salts are semiconductors although salt 1 exhibits a high room temperature conductivity and a semiconducting–semiconducting transition at ca. 150 K which has been attributed to a dimerization in the organic sublattice. © 2002 Elsevier Science (USA)

Key Words: **BEST; BEDS-TTF; TTF; hexacyanometalate; nitroprusside; radical salt; magnetic properties; molecular conductors.**

INTRODUCTION

The most interesting potential of molecular materials nowadays lies on the possibility to create solids in which two or more physical properties, such as conducting, magnetic and optical ones, coexist in the same crystal lattice. This novel class of multifunctional materials should provide the unique opportunity to study the competition and mutual influence of these properties. In the context of the molecular conductors an attractive approach to this goal is to make two–networks solids formed by partially oxidized organic π-electron donor molecules of the tetrathiafulvalene (TTF) family, that support electronic conduction, and charge-compensating complex anions, that can introduce magnetic or optical properties to the solid. So far the most spectacular results dealing with magnetism and conductivitiy are the finding of the first molecular superconductors based upon bis(ethylenedithia)-tetrathiafulvalene (BEDT-TTF) salts with the paramagnetic metal complex anions $[M(ox)_3]^{3-}$ (M^{III} = Fe, Cr; ox = oxalato ligand) (1), the demonstration of an interplay between superconductivity and magnetism in the λ-$(BETS)_2FeCl_4$ phase, (BETS = bis(ethylenedithia)tetraselenafulvalene) (2), and the discovery of coexistence of metal conductivity and ferromagnetism in the layered compound $(BEDT\text{-}TTF)_3[Mn^{II}Cr^{III}(ox)_3]$ (3).

A way of creating molecular conductors incorporating optical properties involves the use of the photochromic nitroprusside complex, $[Fe(CN)_5NO]^{2-}$, as counter-ion in radical cation salts of TTF and its analogs (4). The interest of this anion lies in the fact that it possess extremely long-living metastable excited states at low temperatures that can be generated by laser irradiation (5). These excitations produce important geometrical changes in the anion that may be used to provoke light-induced changes in the packing of the TTF-type counterions and, thus, in their conducting properties.

Most of the work reported so far on the above kind of hybrid salts has been focused on BEDT-TTF, which forms salts with a marked 2D electronic character due to the side-to side connectivity in the derived solids by S···S and C–H···S short contacts. The selenium derivatives of BEDT-TTF can also provide interesting examples of hybrid salts as the substitution of S by the more diffuse Se atom has

[1] To whom correspondence should be addressed. Fax: + 34 96 3864415. E-mail: eugenio.coronado@uv.es.

0022-4596/02 $35.00

often shown an enhancement of the intermolecular chalcogen–chalcogen contacts and hence the conductivity of the solid. Here we report on the synthesis, structural and physical characterization of three new radical salts prepared with the selenium containing donor bis(ethylenediseleno)tetrathiafulvalene (BEST) and the paramagnetic hexacyanoferrate(III) $[Fe(CN)_6]^{3-}$ anion: $(BEST)_4[Fe(CN)_6]$ (**1**) and $(BEST)_3[Fe(CN)_6]_2 \cdot H_2O$ (**2**) and the nitroprusside anion $[Fe(CN)_5NO]^{2-}$: $(BEST)_2[Fe(CN)_5NO]$ (**3**).

EXPERIMENTAL SECTION

Synthesis of the Radical Salts

All the radical salts were synthesized on a platinum wire electrode by the standard electrochemical oxidation of the donor in a U-shaped cell under low constant current ($I = 1-1.2\,\mu A$). The crystallization times vary from 1 to 3 weeks, depending on the salt. The exact conditions for the synthesis of the three radical salts are summarized in Table 1.

X-Ray Crystallographic Analysis

The crystal structure analyses were done on black shiny plate-like single crystals of the three salts (approximate dimensions: $0.50 \times 0.45 \times 0.08\,mm^3$, $0.20 \times 0.20 \times 0.10\,mm^3$ and $0.40 \times 0.20 \times 0.05\,mm^3$ for salts **1**, **2** and **3**, respectively). Relevant crystallographic data and structure determination parameters for the three salts are given in Table 2. Crystallographic data (excluding structure factors) for the structures reported in this paper have been deposited with the Cambridge Crystallographic Data Center as supplementary publication numbers CCDC 183749–183751. Copies of the data can be obtained free of charge on application to CCDC, 12 Union Road, Cambridge CB2 1EZ, UK (Fax: (44) 1223 336-033; E-mail: deposit@ccdc.cam.ac.uk). Cell parameters were obtained by the least-squares refinement method with 25 reflections in the three structures. Intensity data were measured at room temperature on an Enraf-Nonius CAD4 diffractometer with graphite monochromated Mo$K\alpha$ radiation with the ω–2θ method. The measurement of three standard reflections every 120 min revealed no intensity fluctuations The structures were solved by direct methods using the SIR97 program (6), followed by Fourier synthesis and refined on F^2 using the SHELXL-97 program (7). Lorentz, polarization and semiempirical absorption corrections (ψ-scan method) were applied to the intensity data. All calculations were performed in a SPARC station 20 (Sun Microsystems). In **1** and **3** only the heavy atoms (Fe, S and Se) were refined anisotropically. In **2** all the atoms except the H, solvent atoms and the ethylene C atoms of the BEST molecules were refined anisotropically.

A disorder of the NO group is found in the nitroprusside anion of **3**. Thus, the NO group in this anion is delocalized in two of the three independent coordination positions of the Fe atom. These two positions present shorter Fe–C/N bond distances than the other one.

TABLE 1
Synthetic Conditions for the Radical Salts 1, 2 and 3. The Intensity was 1 μA for Salt 1 and 1.2 μA for Salts 2 and 3

Salt	Anode	Cathode
$(BEST)_4[Fe(CN)_6]$	BEST (10 mg)	
(**1**)	$(NEt_4)_3[Fe(CN)_6]$ (70 mg)	$(NEt_4)_3[Fe(CN)_6]$ (70 mg)
	CH_2Cl_2 (8 mL)	CH_2Cl_2 (8 mL)
	CH_3CN (2 mL)	CH_3CN (2 mL)
$(BEST)_3[Fe(CN)_6]_2 \cdot H_2O$	BEST (10 mg)	
(**2**)	$K_3[Fe(CN)_6]$ (100 mg)	$K_3[Fe(CN)_6]$ (100 mg)
	Crown ether (150 mg)	Crown ether (150 mg)
	CH_2Cl_2 (10 mL)	CH_2Cl_2 (10 mL)
	CH_3CH_2OH (2 mL)	CH_3CH_2OH (2 mL)
	H_2O (1 mL)	H_2O (1 mL)
$(BEST)_2[Fe(CN)_5NO]$	BEST (10 mg)	
(**3**)	$Na_2[Fe(CN)_5NO]$ (100 mg)	$Na_2[Fe(CN)_5NO]$ (100 mg)
	Crown ether (150 mg)	Crown ether (150 mg)
	PhCN (10 mL)	PhCN (10 mL)

Conductivity Measurements

DC conductivity measurements over the range 2–300 K were performed by using the magnetometer cryostat with the four or two contacts method (depending on the size of the crystals) on the best developed face of several single crystals of each sample, giving reproducible results in all cases. Contacts to the crystals were made by platinum wires (25 μm diameter) attached with graphite paste to the samples. The cooling and warming rate was 2 K/min in all the measurements.

Magnetic Measurements

Variable temperature susceptibility measurements were carried out in the temperature range 2–300 K at a magnetic field of 1 T on polycrystalline samples with a magnetometer (Quantum Design MPMS-XL-5) equipped with a SQUID sensor. The susceptibility data were corrected from the sample holders previously measured in the same conditions and from the diamagnetic contributions of the salts as deduced by using Pascal's constant tables.

TABLE 2
Crystal Data for the Radical Salts $(BEST)_4[Fe(CN)_6]$ (1), $(BEST)_3[Fe(CN)_6]_2 \cdot H_2O$ (2) and $(BEST)_2[Fe(CN)_5NO]$ (3)

Salt	1	2	3
Formula	$C_{23}H_{16}Fe_{0.5}N_3S_8Se_8$	$C_{21}H_{13}FeN_6S_6Se_6O_{0.5}$	$C_{12.5}H_5Fe_{0.5}N_3S_4Se_4O_{0.5}$
a (Å)	8.889(5)	10.193(3)	6.741(2)
b (Å)	13.241(5)	10.5060(10)	8.868(2)
c (Å)	17.273(5)	17.317(2)	16.098(4)
α (deg)	103.230(5)	87.872(10)	98.15(2)
β (deg)	98.660(5)	72.930(15)	97.52(2)
γ (deg)	107.710(5)	62.16(2)	93.91(2)
V (Å^3)	1831.4(13)	1556.5(5)	940.7(4)
Z	2	2	2
Fw	1250.71	1079.74	677.21
Space group	P-1	P-1	P-1
ρ_{calcd} (g cm^{-3})	2.268	2.303	2.401
λ (Å)	0.71069	0.71069	0.71069
μ (cm^{-1})	8.651	7.931	8.618
Reflns. collected	5280	6049	2210
Reflns. $I > 2\sigma$	2645	2463	1342
θ range (deg)	2.46–28.03	1.24–25.97	2.83–22.50
R^a	0.0922	0.0476	0.0641
R_ω	0.2466^b	0.1108^b	0.1696^b

$^a R = \sum(F_o - F_c)/\sum(F_o)$.
$^b R_\omega = [\sum[\omega(F_o^2 - F_c^2)^2]/\sum[\omega(F_o^2)^2]]^{1/2}$; $\omega = 1/[\sigma^2(F_o^2) + (c_1P)^2 + c_2P]$, where $P = (F_o^2 + 2F_c^2)/3$ with $c_1 = 0.2000$ and $c_2 = 0$ for **1**, $c_1 = 0.0771$ and $c_2 = 0$ for **2** and $c_1 = 0.1514$ and $c_2 = 7.9144$ for **3**.

ESR Measurements

Variable–temperature ESR spectra on polycrystalline samples were recorded at X-band with a Bruker ER200 spectrometer equipped with a helium cryostat. The field was measured using a diphenylpicrylhydrazyl (DPPH, $g = 2.0036$) stable free radical marker.

Electronic spectroscopy

Transmission measurements of pressed KBr pellets were recorded at room temperature with a Perkin-Elmer RX I FT-IR spectrophotometer in the range 400–6000 cm^{-1} and with a Hitachi U-2001 spectrophotometer in the range 9000–28000 cm^{-1} for all compounds.

RESULTS AND DISCUSSION

Synthesis

The three radical salts were obtained by electrochemical oxidation of neutral BEST donor in the presence of the corresponding anion ($[Fe(CN)_6]^{3-}$ or $[Fe(CN)_5NO]^{2-}$). To make soluble these two anions in the corresponding organic solvents, we have followed two different procedures: (i) the use of the NEt_4^+ or NBu_4^+ salts of the anion, and (ii) the addition of a crown ether such as the dibenzo[18]crown[6] to a suspension containing the insoluble Na^+ or K^+ salt of the anion. For $[Fe(CN)_6]^{3-}$ the use of the first method led to the radical salt $(BEST)_4[Fe(CN)_6]$ (**1**) while the use of the second one led to the radical salt $(BEST)_3[Fe(CN)_6]_2 \cdot H_2O$ (**2**). For the $[Fe(CN)_5NO]^{2-}$ anion we have only obtained good-quality single crystals of the radical salt $(BEST)_2[Fe(CN)_5NO]$ (**3**) when using the second procedure.

X-Ray Structures

$(BEST)_4[Fe(CN)_6]$ (1). The structure of this salt consists of alternating layers of organic donors and anions in the *ab* plane (Fig. 1). The organic layer is formed by two crystallographically independent molecules (namely A and B) that are packed in infinite zig-zag chains …AABB… running along the [1$\bar{1}$0] direction (Fig. 2d). The molecular planes of the BEST molecules are all parallel, giving rise to the so-called β phase (Fig. 2a). In contrast to many other β phases, the intrachain S···S distances are shorter than the interchains ones (the shortest intrachain distances are 3.58 and 3.60 Å, compared to 3.66 and 3.80 Å for the interchain ones). The Se···Se distances show the opposite tendency: the intrachain distances are longer than the interchains ones (3.96 and 4.20 Å, compared to 3.63 and 3.66 Å). In summary, there are several S···S, S···Se and Se···Se distances shorter than the sum of the Van der Waals radii (1.80 and 1.90 Å for S and Se, respectively) that confer this salt a marked two-dimensional character in the organic sublattice. There are two different overlapping modes for the BEST molecules: an eclipsed one, between A–B

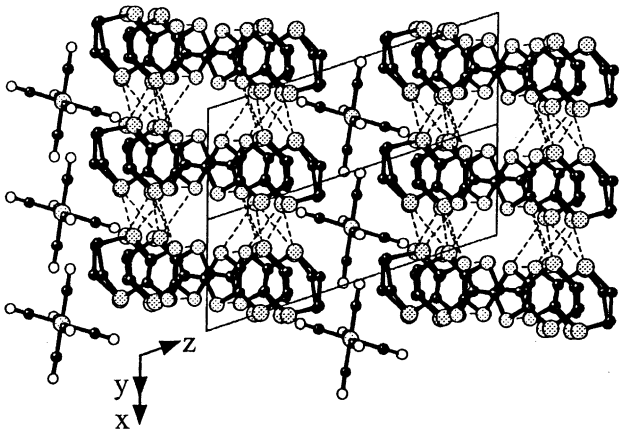

FIG. 1. View down the [1$\bar{1}$0] direction of the structure of **1** showing the alternating organic and inorganic layers. Intermolecular chalcogen-chalcogen short distances are indicated as dotted lines.

molecules (Fig. 2b) and a ring-over-bond mode between A–A and B–B molecules (Fig. 2c). In the first mode, the shortest intermolecular distances (3.58 and 3.60 Å) involve the S atoms, whereas in the second one these are observed between the S atoms of the other (3.82 and 3.86 Å). The low resolution in the bond distances precludes any attempt to estimate the degree of ionicity on each BEST molecule.

The anionic layer is made up of discrete centrosymmetric $[Fe(CN)_6]^{3-}$ anions located in the center of the *bc* face (0, $\frac{1}{2}$, $\frac{1}{2}$), with the Fe(III) ions separated by a minimum distance of 8.89 Å (in the *a* direction). The octahedral $[Fe(CN)_6]^{3-}$ anions are located in the holes left by the organic layers with two of the CN^- ligands pointing towards the organic layer with shortest Se···N contacts of 3.17 and 3.21 Å

$(BEST)_3[Fe(CN)_6]_2 \cdot H_2O$ (2). The structure of this salt consists of two different hybrid organic–inorganic layers (noted I and II) which are interpenetrated and alternate along the *c*-axis (Fig. 3). Layer I is built up from one crystallographically independent BEST (B-type) molecule and one $[Fe(CN)_6]^{3-}$ anion (Fig. 4a), whereas in layer II there are two (A-type) BEST molecules per anion (Fig. 4b), giving an overall stoichiometry of three BEST molecules (two A and one B-type) and two $[Fe(CN)_6]^{3-}$ anions. The structure can also be described as consisting of hybrid layers in the *ac* plane (noted III) separated by $[Fe(CN)_6]^{3-}$ anions that also penetrate the hybrid layers (Fig. 3). These hybrid layers are formed by one A-type and two B-type BEST molecules packed surrounding the $[Fe(CN)_6]^{3-}$ anions in a square arrangement (Fig. 4c). The angle between the average planes through the TTF moieties of the A- and B-type BEST molecules is 41.6°. The interpenetration of the layers gives rise to many short

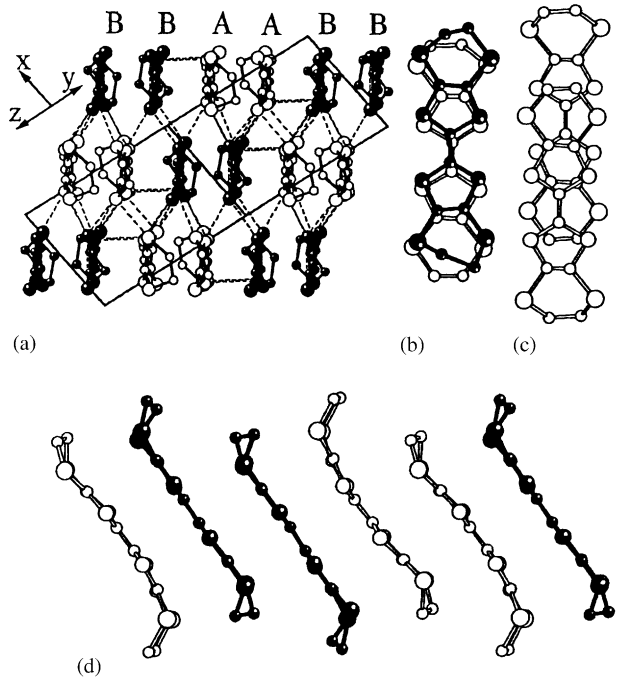

FIG. 2. Views of the structure of **1**: (a) The organic layer showing the β packing of the BEST molecules. Intermolecular chalcogen–chalcogen short distances are indicated as dotted lines. (b) Eclipsed overlapping between the A- and B-type BEST molecules. (c) Ring-over-bond overlapping between A–A and B–B BEST molecules. (d) The organic chains running along the [1$\bar{1}$0] direction. A- and B-type molecules are represented in white and black, repectively.

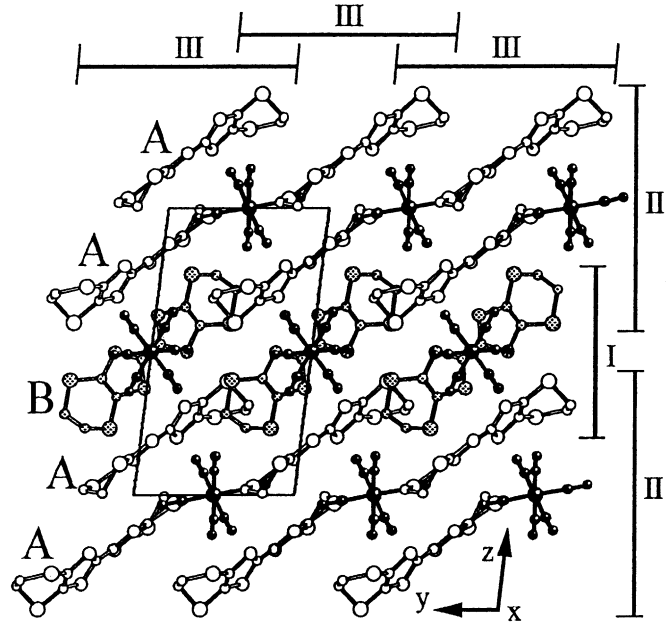

FIG. 3. View of the *bc* plane showing the interpenetrated hybrid layers (I and II, parallel to the *ab* plane and III, parallel to the *ac* plane) in **2**. A- and B-type molecules are represented in white and gray, respectively.

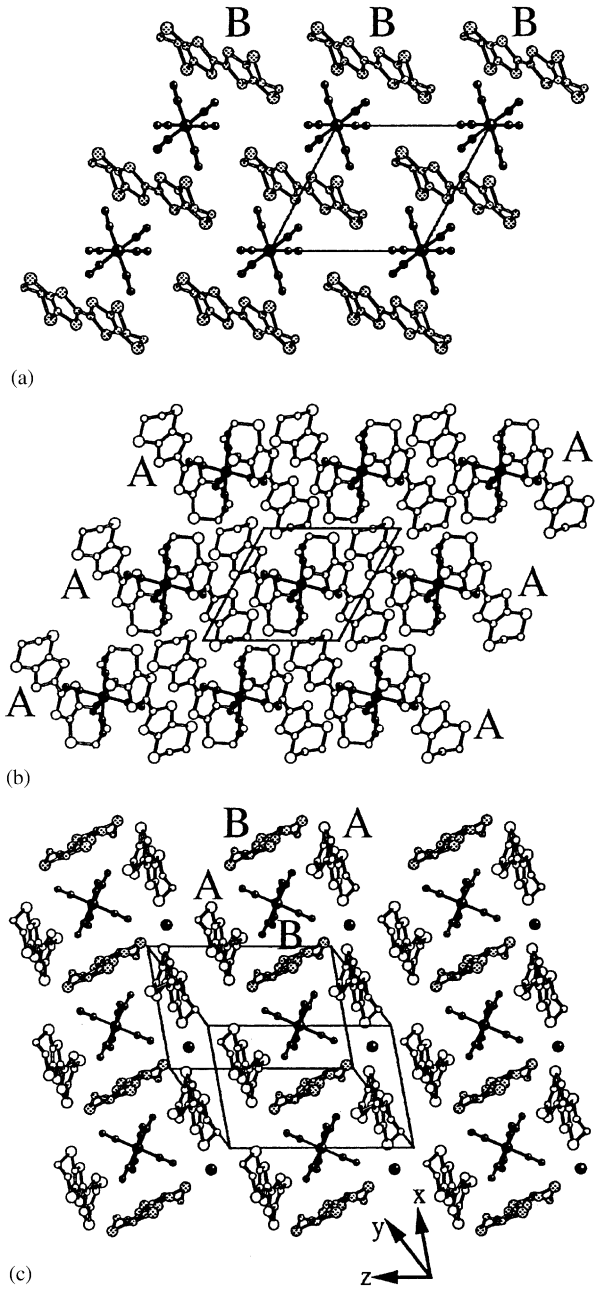

FIG. 4. Views of the structure of **2**: (a) type I layer in the *bc* plane. (b) type II layer in the *bc* plane. (c) type III layer showing the $[Fe(CN)_6]^{3-}$ anions of the layer surrounded by four BEST molecules in a square arrangement. Only the Fe atom of the $[Fe(CN)_6]^{3-}$ anions that separate the layers is showed. A- and B-type molecules are represented in white and gray, respectively.

intermolecular contacts in all the directions which confers this structure a marked three-dimensional character. Thus, the shortest intermolecular Se···S distances are 3.76 Å inside the type II layers and 3.52 Å between layers I and II. This three-dimensional character is quite unusual in radical salts based on TTF–type donors, and even more when the counterion is a relatively small octahedral anion. In fact, the very few examples of three–dimensional structures known to date contain bulky polyanions that are believed to impose their close-packing trends (8).

The inorganic sublattice is formed by two crystallographically centrosymmetric independent $[Fe(CN)_6]^{3-}$ anions located in the center of the *c*-axis (0, 0, $\frac{1}{2}$) and in the center of the *ab* face ($\frac{1}{2}$, $\frac{1}{2}$, 0). The shortest Fe–Fe distance (between two crystallographically different Fe atoms) is 9.00 Å. The interpenetration between organic and inorganic layers also gives rise to many short anion-donor contacts (shortest S···N and Se···N distances of 3.34 and 3.10 Å, respectively). The water molecule is located between the BEST molecules and the $[Fe(CN)_6]^{3-}$ anions, with shortest S···O_w, Se···O_w and N···O_w distances of 3.10, 3.32 and 2.84 Å, respectively.

Still the most surprising feature of this salt is the high oxidation state of the organic donor. In fact, owing to the stoichiometry of the salt (3:2) and the charge of the hexacyanoferrate anion (−3), the BEST molecules should present a degree of ionicity of +2. An additional proof of this unusual oxidation state comes from the resemblance of the bond distances of the central TTF skeleton of the BEST molecules in **2** and those found in the few examples of radical salts with dicationic BEDT-TTF molecules (Table 3).

(BEST)$_2$[Fe(CN)$_5$NO] (3). The structure of this salt closely resembles that of **1** (Figs. 5 and 6). The main differences are that now the stoichiometry is 2:1 instead of 4:1 and that there is only one crystallographically independent BEST molecule. The organic and inorganic layers alternate in the *c* direction (Fig. 5). The organic layers present also a β-packing (Fig. 6a) with the zig-zag chains running along the *b*-axis (Fig. 6d). As in salt **1**, the shortest interchains contacts involve Se atoms (3.54 and

TABLE 3
Comparison of the Estimated Charges Form the Bond Distances in Neutral BEDT-TTF, Dicationic BEDT-TTF and the BEST Molecules in 2

Salt	Mol.	a^a	b^b	Q^c	Ref.
BEDT-TTF (ET)		1.312	1.757	0	15
$(ET)[ClO_4]_2$		1.439	1.683	2.11	16
$(ET)_3[ZnCl_4]_2$		1.438	1.680	2.13	17
$(ET)_5[Hg_5Br_{11}]$		1.43	1.68	2.02	18
$(BEST)_3[Fe(CN)_6]_2H_2O$ (**2**)	A	1.43(1)	1.68(1)	2.02	This work
	B	1.45(2)	1.69(1)	2.18	This work

[a] Central C = C bond distance.
[b] Mean central C–S bond distance.
[c] Q = charge estimated with the formula $Q = -17.92 + 23.43*(a/b)$ from Ref. 19.

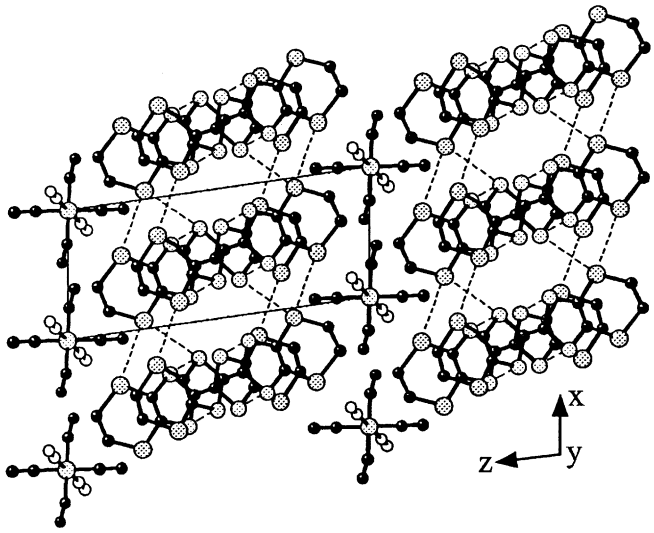

FIG. 5. View down the *b* direction of the structure of **3** showing the alternating organic and inorganic layers. The four possible locations of the NO group are indicated in black. Intermolecular chalcogen–chalcogen short distances are indicated as dotted lines.

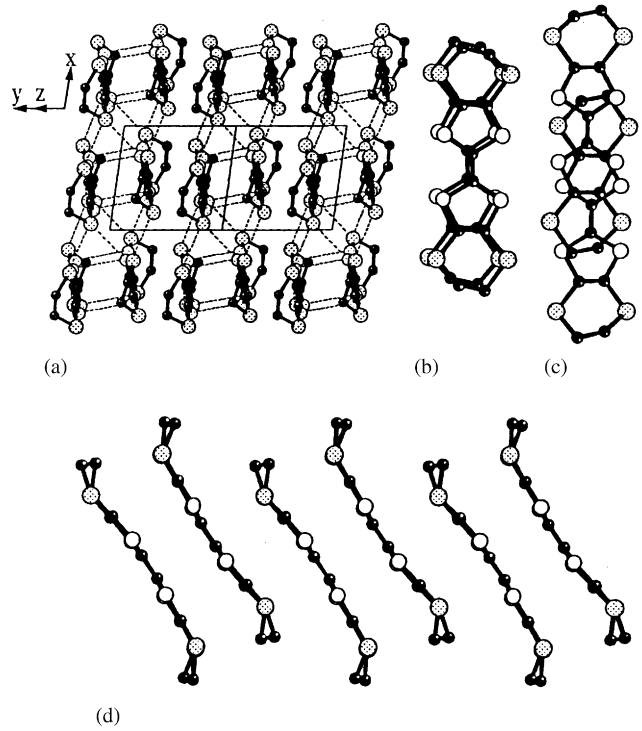

FIG. 6. Views of the structure of **3**: (a) The organic layer showing the β packing of the BEST molecules. Intermolecular chalcogen–chalcogen short distances are indicated as dotted lines. Eclipsed overlapping **(b)** and ring-over-bond overlapping (c) between the BEST molecules. (d) The organic chains running along the [010] direction.

3.62 Å) and the intrachain ones involve S atoms (3.52 Å), leading to a marked two-dimensional character for the salt (Fig. 6a). In **3**, there are also two different overlapping modes (eclipsed and ring-over-bond, Figs. 5b and 5c) whose shortest intermolecular distances (3.52 and 3.76 Å) involve S···S and Se···S contacts, respectively.

The inorganic layer is formed by discrete centrosymmetric $[Fe(CN)_5NO]^{2-}$ anions located in the corners of the unit cell. The anions present a positional disorder of the NO ligand that is delocalized in two of the three independent coordination positions of the Fe atom. The positional disorder of the NO ligand is confirmed by the bond distances between the Fe atom and the surrounding atoms. Thus, there are two independent short Fe–N/C bond distances (1.79 and 1.82 Å), which are in between the Fe–C and the Fe–N bond distances in the $[Fe(CN)_5NO]^{2-}$ anion (1.92–1.94 and 1.65–1.67 Å, respectively) (9). The Fe–C bond distance of the other independent position is longer (1.96 Å) and very close to those found in the Fe–C bonds of the ordered $[Fe(CN)_5NO]^{2-}$ anion (1.92–1.94 Å) (9). The Fe–N–O angles are 166° and 178° for both disordered positions. One of the two positions for the NO groups is located between the organic layers, whereas the other one penetrates the organic layers with a shortest N/O···Se distance of only 3.14 Å. This distance is much shorter than the sum of the Van der Waals radii of the atoms (3.45 Å) suggesting the existence of anion–cation interactions in this salt.

From the stoichiometry of the salt (2:1) and the charge of the inorganic anion (−2) we can conclude that the BEST molecules are charged +1.

Electronic Spectroscopy

The IR spectra of all the radical salts show the typical bands of the anions (the CN band appears at 2111 cm^{-1} in **1**, 2095 cm^{-1} in **2** and 2139 cm^{-1} in **3**, where there is also another band at 1940 cm^{-1} coming from the NO group of the nitroprusside anion) (9a). As far as the donors are concerned, the IR spectra show some important differences from one salt to another. Thus, the ν_3 and ν_{27} bands, corresponding to the central C=C bond, appear, respectively, at 1356 and 1442 cm^{-1} in **1**, at 1364 and 1499 cm^{-1} in **2** and at 1344 and 1450 cm^{-1} in **3**. These bands are sensitive to the degree of ionicity of the donor molecules (10), so that the observed differences are consistent with the different formal degrees of ionicity of the BEST molecules in the three salts (+3/4 in **1**, +2 in **2** and +1 in **3**). Still, for **1** both ν_3 and ν_{27} bands appear at values which are very close to those of **3**, suggesting the presence of BEST molecules with a degree of ionicity of +1. This possibility would imply the presence of totally charged molecules (+1) coexisting with other partially ionized ones (+0.5), and is in agreement with the UV–vis spectrum (see below). As there are two crystallographically independent BEST molecules (noted A and B) and there

are two molecules of each type per anion, this charge distribution would give a total cationic charge of +3 for the four BEST molecules, in agreement with the anionic charge (−3).

In the UV–vis–NIR spectrum of **1**, one can observe a broad and intense charge transfer band centered in the IR region at approx. 6000 cm^{-1}, called A band, which is the signature of the mixed valence state in the donor molecules, together with a weaker band, at 11670 cm^{-1}, the so-called B-band, corresponding to an electronic transfer between completely ionized donor molecules (11). Salts **2** and **3** only show the B-band which are centered at 11325 cm^{-1} and 11700 cm^{-1}, respectively. Such an observation clearly indicates that in these two salts the BEST molecules are completely ionized, as deduced from the stoichiometry.

Electrical Properties

The electrical conductivity of **1** was measured on six different single crystals of various dimensions. Depending on the size of the crystal, 2 or 4 contacts were attached to the best developed face of the crystal. Very similar values of the room temperature conductivity and identical thermal dependencies were observed in all cases. Fig. 7 shows the typical thermal variation of one of the samples measured by the four contacts method. A high conductivity ($\approx$11 S cm^{-1}) is observed at room temperature that decreases when decreasing temperature, indicating a semiconducting behavior with an activation energy of $\approx$25 meV in the region 160–300 K. Below $\approx$160 K, the decrease in the conductivity is more pronounced in all the measured samples. In fact, a change in the slope of the logarithm of the conductivity vs 1000/T is observed at this temperature (inset in Fig. 7) leading to an increase in the activation energy in this region ($\approx$35 meV). Such a result suggests a semiconducting-to-semiconducting transition and is also observed in the thermal variation of the spin susceptibility of the organic sublattice, as deduced from the ESR measurements (see below). Salts **2** and **3** present very low room temperature conductivities ($\approx 10^{-6}$ and $\approx 2.10^{-7}$ S cm^{-1}, respectively) and semiconducting thermal behaviors, as expected for a packing of totally ionized donor molecules.

Magnetic Properties

The product of the magnetic susceptibility times the temperature ($\chi_m T$) as a function of the temperature for the three salts are displayed in Fig. 8 together with those of the NEt_4^+ and $AsPh_4^+$ salts of the $[Fe(CN)_6]^{3-}$ anion. At room temperature, the $\chi_m T$ product of the radical salts containing the paramagnetic $[Fe(CN)_6]^{3-}$ anion (salts **1** and **2**) is, respectively, 0.85 and 0.81 emu K mol^{-1} and continuously decreases upon cooling down to reach a value of 0.49 and 0.37 emu K mol^{-1} at 2 K. Such behaviors are dominated by the magnetic properties of the $[Fe(CN)_6]^{3-}$ anion. In this complex, the Fe(III) is a low-spin d^5 configuration, being then described by an orbitally degenerate term $^2T_{2g}$. This orbital contribution leads to a magnetic behavior characterized by a strong magnetic anisotropy and by a temperature-dependent $\chi_m T$ product that varies from salt to salt. In fact with bulk cations such as NEt_4^+ or $AsPh_4^+$, the $\chi_m T$ product decreases from values

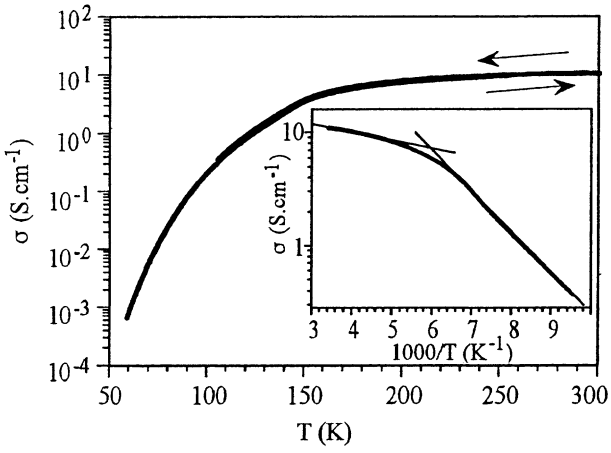

FIG. 7. Thermal variation of the electrical conductivity in **1**. Inset: logarithmic plot of the conductivity as a function of $1000/T$ showing the change in the slope at about 160 K.

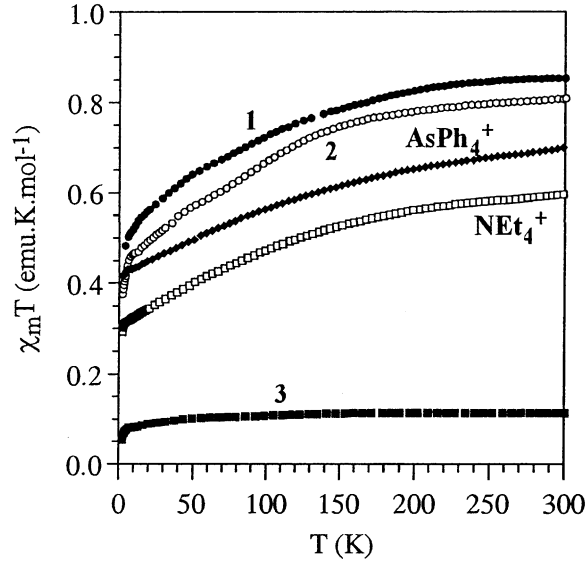

FIG. 8. $\chi_m T$ vs T plot of the salts **1** (filled circles), **2** (empty circles), **3** (filled squares) and of the NEt_4^+ (empty squares) and $AsPh_4^+$ (filled rhombs) salts of the $[Fe(CN)_6]^{3-}$ anion.

of 0.6–0.7 emu K mol^{-1} to values of 0.3–0.4 emu K mol^{-1} at low temperatures (Fig. 8). Hence, from these magnetic data, it is very difficult to extract any information on the magnetic contribution coming from the organic sublattice. Salt **3**, which contains the diamagnetic $[Fe(CN)_5NO]^{2-}$ anion, presents a constant and very low value of the $\chi_m T$ product (approx. 0.1 emu K mol^{-1}), suggesting that the organic sublattice does not contribute to the magnetic moment of salt **3** and therefore, that the two electrons per formula in the BEST molecules must be strongly antiferromagnetically coupled. The weak Curie-tail observed (0.1 emu K mol^{-1}) can be attributed to the presence of a small amount of isolated $(BEST)^+$ radicals in the lattice due to crystalline defects and to the charge localization effects taking place in these semiconductors at low temperature as has already been observed in other radical salts of TTF-type donors (12).

ESR Measurements

In order to obtain a more precise information on the magnetic contribution of the organic sublattices in all the salts, specially in salts **1** and **2**, we have performed ESR measurements for the three salts. Salt **1** presents a very wide ESR signal with a line width of 1800 G coming from the $[Fe(CN)_6]^{3-}$ anion. This signal can already be seen at room temperature and remains almost unchanged down to 4.2 K, indicating the absence of any strong interaction among the $[Fe(CN)_6]^{3-}$ anions, as expected from the structure. Besides this wide signal, one can also see a narrow symmetrical signal coming from the organic radicals centered at $g = 2.0060$ with a line width of 65 G at room temperature. This signal increases its intensity with decreasing temperature down to approx. 200 K (Figs. 9 and 10). Below this temperature, the intensity of this signal decreases with decreasing temperature and at about 60 K it splits into two narrow signals centered at $g = 1.9959$ and 2.0081 with line widths of approx. 15 and 7 G, respectively. These two narrow lines follow a Curie law when decreasing the temperature. This behavior can be reproduced with the Bleaney–Bowers model for an antiferromagnetically coupled dimer, giving a singlet-to-triplet gap of $\Delta/k_B \approx 170\,cm^{-1}$ (solid line in Fig. 10). The low temperature behavior can be well reproduced with a Curie-tail term ($\chi = C/T$) (solid line in Fig. 10).

The splitting of the signal coming from the BEST molecules into two weaker and narrower signals suggests the presence of a structural transition that starts at about 100 K (temperature at which the two signals appear) and is accomplished at about 60 K (when the original signal has disappeared). This broad transition may produce an increase in the number of crystallographically independent molecules and a decrease in the dimensionality of the salt.

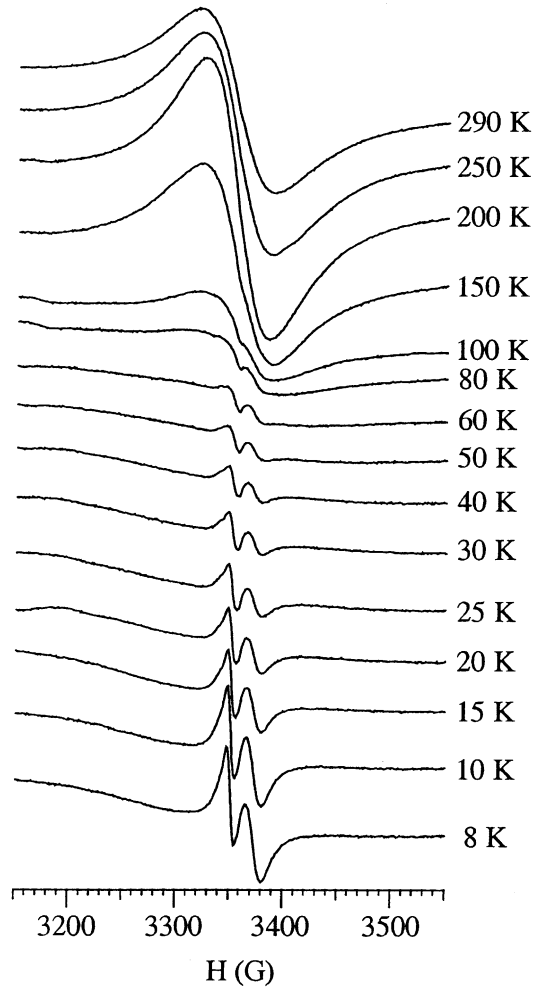

FIG. 9. ESR spectra at different temperatures of the salt **1**.

This transition is not detected by the static susceptibility measurements as it is probably masked by the stronger magnetic moment of the $[Fe(CN)_6]^{3-}$ anions. A similar transition was observed in the κ phase of the BEDT-TTF salt of the same anion (13).

Interestingly, the line width at room temperature of the ESR signal coming from the BEST molecules is very high for a β phase (the typical values for the line widths are in the range 15–25 G) (14). This unusual result may be attributed to a possible decrease in the spin relaxation time due to two factors: (i) The presence of many intra and interchain short contacts between the S and Se atoms; and (ii) The presence of the paramagnetic anions $[Fe(CN)_6]^{3-}$, very close to the BEST molecules, which may provide additional pathways for the spin relaxation. In fact, a similar behavior was observed in the salt β-(BEDT–TTF)$_5$[Fe(CN)$_6$]$\cdot$10H$_2$O (13).

The ESR spectrum of salt **2** is very similar to that of salt **1** although now the signal coming from the organic

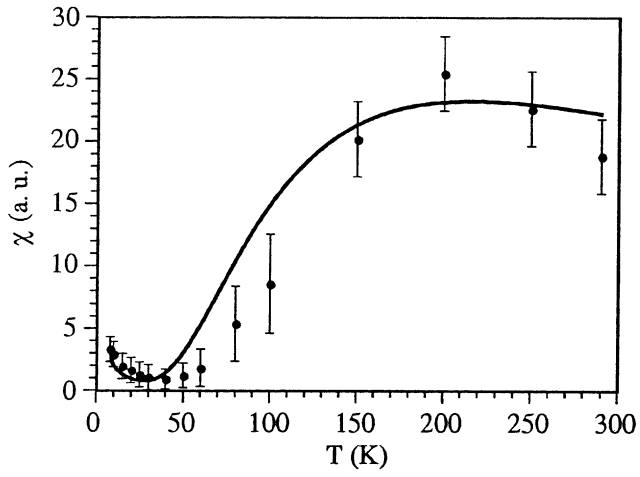

FIG. 10. Thermal variation of the spin susceptibility of salt **1** derived from the area of the narrow ESR signal coming from the organic radicals.

sublattice (at $g = 2.0087$ with a line width of 13 G) is very weak compared with that of the anion (ratio 1:100). Its thermal behavior follows the Curie law, suggesting that this signal comes from isolated $(BEST)^+$ radicals due to crystal defects and, thus, that the organic sublattice has no contribution to the magnetic moment of this salt. This result fully agrees with the diamagnetic character of the organic sublattice as it is formed by close-shell dicationic BEST molecules.

Salt **3** also presents a narrow and very weak ESR signal at $g = 2.0070$ with a line width of 18 G that follows the Curie law. As in the previous case, this signal comes from a small amount of paramagnetic impurities of $(BEST)^+$ radicals dispersed now in an antiferromagnetic lattice of strongly coupled $BEST^+$ radicals. This result is in agreement with the static susceptibility data. On the other hand, the diamagnetic $[Fe(CN)_5NO]^{2-}$ anion is ESR silent and no signal arising from the inorganic sublattice has been detected.

Final Discussion

In this contribution, we have shown the possibility of combining the selenium–containing organic donor BEST with the magnetic anion $[Fe(CN)_6]^{3-}$ and the photochromic nitroprusside anion $[Fe(CN)_5NO]^{2-}$. Three novel radical salts have been obtained namely: $(BEST)_4[Fe(CN)_6]$ (**1**), $(BEST)_3[Fe(CN)_6]_2 \cdot H_2O$ (**2**) and $(BEST)_2[Fe(CN)_5NO]$ (**3**). From a synthetic point of view, it is interesting to note that for the BEST/$[Fe(CN)_6]^{3-}$ system, the fact of obtaining two different radical salts when using the K^+ or the NEt_4^+ salts of the $[Fe(CN)_6]^{3-}$ anion that have different structures and stoichiometries has to be attributed to the different available free anion concentration for each synthetic method. Thus, the use of a low-soluble salt of the anion (as for example the salt $K_3[Fe(CN)_6$) leads to a low concentration of free anions in the cell which results in a high applied potential during the electrochemical oxidation of the organic donor, as the reaction is carried out at a constant current. Such a feature favors the full oxidation of the organic donor. This situation is exemplified by salt **2** in which the high potential is even able to produce the second oxidation of the BEST molecules. Notice that a charge of $+2$ for an organic donor is very unusual in the radical salts of the TTF-type (only a few salts of BEDT-TTF present this high charge, see Table 3) and completely new for BEST. When using a very soluble salt of the anion (as for example the NEt_4^+ salt), the oxidation state of the donor can be much lower. This is the case of salt **1** which exhibits a mixed valence state in the organic donors with an average charge of $\frac{3}{4}$.

From a structural point of view, the most remarkable feature has been the observation of a 3D packing in **2** with short contacts between BEST molecules of different layers. To the best of our knowledge there is only a precedent of a 3D packing for BEST. It has been observed in the salt $(BEST)_3[PMo_{12}O_{40}]$ containing the bulky Keggin anion (8b). The other two salts (**1** and **3**) exhibit a typical layer structure with identical packings of the organic donors, even if the anionic charge is different in these two cases (-3 in **1** and -2 in **3**). Such a result emphasizes the tendency of BEST to adopt a β-packing motif when an octahedral metal complex is used as charge compensating ion. The only significant difference between these two salts is observed in the different stoichiometries (4:1 and 2:1 in **1** and **3**, respectively). In fact, if we compare the anionic layers in both structures, we can see that in salt **1** one half of the anionic positions of salt **3** are empty. An interesting possibility derived from this observation would be the synthesis of a 4:1 salt with the $[Fe(CN)_5NO]^{2-}$ anion, as this salt would have a partial ionization degree of $\frac{1}{2}$ in the organic donors. Attempts to prepare this salt starting with the NEt_4^+ precursor are in progress.

The charge distribution in the organic donors of the three salts is another important point that deserves some attention. From the stoichiometries and anionic charges, it seems clear that in **2** and **3** the charge on each donor molecule must be $+2$ and $+1$, respectively, in agreement with the electronic and IR spectra, the bond distance analysis (Table 3) and magnetic properties. In **1**, where the average charge per donor molecule is $+3/4$, the charge distribution is more difficult to establish. As the total charge per formula of the organic network is $+3$, a plausible possibility should involve a charge of $+1$ for the A-type molecules and of $+0.5$ to the B-type molecules. The differences in the intradimer distances are in agreement with such a distribution. Thus, the average Se···S distances are 3.75 Å between B molecules and 3.90 Å between A molecules, suggesting that the A-type molecules bear a

higher charge. The proposed distribution helps to explain the magnetic and conducting properties of this salt. Thus, assuming that the charge of the A and B molecules is $+1$ and $+0.5$, respectively, the organic sublattice can be viewed as formed by two types of parallel chains of dimers running along the *a* direction: a chain of BB dimers containing one electron per dimer $(BEST)_2^+$ and a chain of AA dimers with two localized electrons per dimer $(BEST^+)_2$ that are strongly antiferromagnetically coupled (as observed in **3**). The existence of the chains of dimers is supported by the presence of very short Se···Se contacts between the BB dimers (and also between the AA dimers) along the *a* direction: 3.63 Å (and 3.73 Å) compared to 3.8 Å, which is the sum of the Van der Waals radii of the Se atoms (Fig. 2a). The abrupt change in the conducting and magnetic properties observed at approx. 160 K can be attributed to a dimerization along the chain formed by the BB dimers that would give rise to a charge localization and therefore to a decrease in the conductivity and to an enhancement in the antiferromagnetic coupling of the localized spins.

ACKNOWLEDGMENTS

This work was supported by the Spanish Ministerio de Ciencia y Tecnología (Grants 1FD97–1765 and MAT2001-3507) and the European Union (TMR-Network on molecular magnetism: from materials to the devices).

REFERENCES

1. M. Kurmoo, A. W. Graham, P. Day, S. J. Coles, M. B. Hurtshouse, J. L. Caulfield, J. Singleton, F. L. Pratt, W. Hayes, L. Ducasse, and P. Guionneau, *J. Am. Chem. Soc.* **117,** 12209 (1995).
2. H. Kobayashi, H. Tomita, T. Naito, A. Kobayashi, F. Sakai, T. Watanabe, and P. Cassoux, *J. Am. Chem. Soc.* **118,** 368 (1996).
3. E. Coronado, J. R. Galán-Mascarós, C. J. Gómez-García, and V. N. Lauhkin, *Nature* **408,** 447 (2000).
4. (a) H. Yu, and D. Zhu, *Physica C* **282–287,** 1893 (1997); (b) M. Gener, E. Canadell, S. S. Khasanov, L. V. Zorina, R. P. Shibaeva, L. A. Kushch, and E. B. Yagubskii, *Solid State Commun.* **111,** 329 (1999); (c) L. A. Kushch, L. Buravov, V. Tkacheva, E. B. Yagubskii, L. Zorina, S. Khasanov, and R. Shibaeva, *Synth. Met.* **102,** 1646 (1999); (d) M. Clemente-León, E. Coronado, J. R. Galán-Mascarós, C. J. Gómez-García, and E. Canadell, *Inorg. Chem.* **39,** 5394 (2000); (e) M. Clemente-León, E. Coronado, J. R. Galán-Mascarós, C. Giménez-Saiz, C. J. Gómez-García, E. Ribera, J. Vidal-Gancedo, C. Rovira, E. Canadell, and V. N. Laukhin, *Inorg. Chem.* **40,** 3526 (2001); (f) M. E. Sanchez, M. L. Doublet, C. Faulmann, I. Malfant, P. Cassoux, L. A. Kushch, and E. B. Yagubskii, *Eur. J. Inorg. Chem.* (2001) 2797; (g) L. V. Zorina, S. S. Khasanov, R. P. Shibaeva, M. Gener, R. Rousseau, E. Canadell, L. A. Kushch, E. B. Yagubskii, O. O. Drozdova, and K. Yakushi, *J. Mater. Chem.* **10,** 2017 (2000).
5. M. D. Carducci, M. R. Pressprich, and P. Coppens, *J. Am. Chem. Soc.* **119,** 2669 (1997).
6. SIR97: A. Altomare, M. C. Burla, M. Camalli, G. Cascarano, C. Giacovazzo, A. Guagliardi, A. G. G. Moliterni, G. Polidori, and R. Spagna, *J. Appl. Crystallogr.* **32,** 115 (1999).
7. G. M. Sheldrick, University of Göttingen, Göttingen, Germany, 1997.
8. (a) E. Coronado, J. R. Galán Mascarós, C. Gimenez-Saiz, C. J. Gómez-García, C. Rovira, J. Tarrés, S. Triki, and J. Veciana, *J. Mater. Chem.* **8,** 313 (1998); (b) E. Coronado, J. R. Galán-Mascarós, C. Giménez-Saiz, C. J. Gómez-García, L. R. Falvello, and P. Delhaes, *Inorg. Chem.* **37,** 2183 (1998).
9. (a) H. L. Shyu, H. H. Wei, and Y. Wang, *Inorg. Chim. Acta* **258,** 81 (1997); (b) M. R. Pressprich, M. A. White, Y. Vekhter, and P. Coppens, *J. Am. Chem. Soc.* **116,** 5233 (1994).
10. (a) M. E. Kozlov, K. I. Pokhodnia, and A. A. Yurchenko, *Spectrochim. Acta, Part A* **45,** 437 (1989); (b) R. Swietlik, C. Garrigou-Lagrange, C. Sourisseau, G. Pages, and P. Delhaès, *J. Mater. Chem.* **2,** 857 (1992).
11. J. A. Torrance, B. A. Scot, and F. B. Welber, *Phys. Rev. B: Condens. Matter* **19,** 730 (1979).
12. (a) C. Bellito, M. Bonamico, and G. Staulo, *Mol. Cryst. Liq. Cryst.* **232,** 155 (1993); (b) C. J. Gómez-García, C. Giménez-Saiz, S. Triki, E. Coronado, P. Le Magueres, L. Ouahab, L. Ducasse, C. Sourisseau, and P. Delhaes, *Inorg. Chem.* **34,** 4139 (1995); (c) C. Bellito, M. Bonamico, V. Fares, F. Federici, G. Righini, M. Kurmoo, and P. Day, *Chem. Mater.* **7,** 1475 (1995); (d) E. Coronado, J. R. Galán-Mascarós, C. Giménez-Saiz, C. J. Gómez-García, and S. Triki, *J. Am. Chem. Soc.* **120,** 4671 (1998).
13. P. Le Magueres, L. Ouahab, P. Briard, J. Even, M. Bertault, L. Toupet, J. Ramos, C. J. Gómez-García, and P. Delhaes, *Mol. Cryst. Liq. Cryst.* **305,** 479 (1997).
14. J. M. Williams, J. R. Ferraro, R. J. Thorn, K. D. Carlson, U. Geiser, H. H. Wang, A. M. Kini, and M. H. Whangbo, "Organic Superconductors. Synthesis, Structure, Properties and Theory." Prentice–Hall, Englewood Cliffs, NJ, 1992.
15. H. Kobayashi, A. Kobayashi, Y. Sasaki, G. Saito, and H. Inokuchi, *Bull. Chem. Soc. Jpn.* **59,** 301 (1986).
16. K. A. Abboud, M. B. Clevenger, G. F. Oliveira, and D. R. Talham, *J. Chem. Soc. Chem. Commun.* (1993) 1560.
17. V. E. Korotkov, and R. P. Shibaeva, *Sov. Phys. Crystallogr. (Engl. Transl.)* **34,** 865 (1989).
18. T. Mori, P. Wang, K. Imaeda, T. Enoki, and H. Inokuchi, *Solid State Commun.* **64,** 733 (1987).
19. Although this formula has been developed for the BEDT-TTF donor, it seems to be valid for the BEST molecule as the central TTF skeleton remains unchanged. T. C. Umland, S. Allie, T. Kuhlmann, and P. Coppens, *J. Phys. Chem.* **92,** 6456 (1987).